

Integral Human Pose Regression

Xiao Sun¹, Bin Xiao¹, Shuang Liang^{2*}, Yichen Wei¹

¹Microsoft Research, ² Tongji University

{xias, bixi, yichenw}@microsoft.com, shuangliang@tongji.edu.cn

Abstract

State-of-the-art human pose estimation methods are dominated by complex multi-stage architectures using a heat map representation. The representation has a few issues in nature, such as no end-to-end training, quantization error and sensitivity to multiple modes.

While pose estimation is essentially a regression problem, existing regression approaches are not as effective. This work proposes an integral regression approach that unifies the heat map representation and joint regression, thus possessing the merits of both paradigms. It is differentiable and allows end-to-end training. It is simple, fast, and compatible with any heat map based methods. Comprehensive experiments verify its efficacy. Building upon simple baseline networks, its performance on benchmarks is strong and competitive to state-of-the-art.

1. Introduction

Human pose estimation has been extensively studied for years and seen significant progresses recently using deep convolutional neural networks. An interesting observation is that all state-of-the-art methods [43, 5, 29, 4, 15, 19, 12, 10, 8, 32, 16] adopt the heat map representation. Specifically, each heat map encodes the likelihoods of all locations being a specific joint. Given a learnt heat map, the joint is predicted as the location with the *maximum likelihood*.

In spite of its good performance, a heat map representation bears a few drawbacks in nature. The “taking-maximum” operation is not differentiable and prevents the train from end-to-end. A heat map has smaller resolution than that of input image. This causes inevitable quantization errors. A heat map is learnt via per-pixel classification. Thus, it usually presents multiple local modes and makes the “taking-maximum” operation unstable and error prone.

To alleviate above issues, a multi-stage architecture is adopted in many state-of-the-art methods [43, 29]. The heat maps from the previous stage are used as input for the next

stage. The contextual information from different joints is exploited to enhance the heat map prediction as more stages are used. While such approaches achieve good accuracy, the networks are complex and computationally demanding (e.g., see Table 7).

From another viewpoint, pose estimation is essentially a regression problem. A regression approach performs end-to-end learning and produces continuous output. It avoids the issues above. However, regression methods are much less popular, because they are harder to train than heat maps and harder to use in a multi-stage architecture.

This work presents a simple approach that unifies the heat map representation and joint regression. It modifies the “taking-maximum” operation to “taking-expectation”. The joint is estimated as the integration of all locations in the heat map, weighted by their probabilities (normalized from likelihoods). We call this approach *integral regression*. It shares the merits of both heat map representation and regression approaches, while avoiding their drawbacks. The integral function is differentiable and allows end-to-end training. It is simple and brings little overhead in computation and storage. It can be easily combined with *any* heat map based methods.

Comprehensive experiments verify that integral pose regression is effective under various settings, indicating that the effectiveness is due to the integral representation. While our results are built upon simple baseline networks, the performance is strong and competitive to the state-of-the-art on challenging benchmarks [2, 23].

2. Related Works

Human pose estimation has been extensively studied for years. A complete review is beyond the scope of this work. We refer the readers to [26, 37] for a detailed survey.

Heat map based methods It is crucial to model the dependency between different joints/heat maps to obtain good accuracy for such methods. Some works design complex network structures to learn such dependency. Chu et al. [11] introduce a geometrical transform kernels together with a bi-directional tree structured model in CNN framework that

*Corresponding author.

can pass informations between different joint heat maps. Yang et al. [44] design sophisticated message passing layers for conducting inference and learning on mixture of parts with deformation constraints between parts.

Most recent successful methods adopt a common multi-stage architecture [43, 5, 29, 4, 15, 19, 12, 10, 8, 32]. The results of the previous stage are used as inputs to enhance or regularize the learning of the next stage. Wei et al. [43] design a six-stage sequential architecture composed of convolutional networks that directly operate on heat maps from previous stages. The ambiguity of heat maps reduces iteratively using more stages with large respective field. Newell et al. [29] also introduce an eight-stage stacked hourglass architecture using even more sophisticated network design which combines multi-resolution hierarchy features that better capture the various spatial relationships associated with the body. Chu et al. [12] further extend hourglass [29] with a multi-context attention mechanism. In each stack of hourglass, they generate extra multi-resolution attention maps and also apply an extra multi-semantic attention map. More recently, Chen et al. [8] also extend hourglass by learning extra discriminators to distinguish the real poses from the fake ones. Those discriminators need more hourglass stages and the training of the network follows the sophisticated strategy of conditional Generative Adversarial Networks (GANs).

A multi-stage architecture effectively reduces ambiguity in the heat map and encodes joint dependency implicitly. However, it also increases the network and computation complexity.

Joint regression Toshev et al. [42] firstly apply CNNs on human pose estimation task and formulate it as a holistic joint location regression problem. They argue that regression can naturally provides better holistic reasoning of the pose by regression than part detection models. Meanwhile, they also find that *a one-shot holistic regression only learns filters capturing pose properties at coarse scale which is insufficient to always precisely localize the body joints*. Hence, cascaded pose regressor that iteratively refine the one-shot holistic regression result using local image patch is introduced to further improve the result. Carreira et al. [6] propose a multi-stage self-correcting model that progressively changes an initial solution by feeding back error predictions instead of one-shot holistic regression. Recently, Sun et al. [38] find it helpful to reformulate the pose representation as bones instead of joints and then enhance the loss function.

Regression methods directly output the continuous joint coordinates and naturally solve the heat map ambiguity problem. However, their performance is usually inferior. This is because regression is harder to train than heat maps and hard to use in a multi-stage architecture.

$k \in \{1, 2, \dots, K\}$	joint index
$\mathbf{J} = \{\mathbf{J}_k\}$	joints
$\mathbf{H} = \{\mathbf{H}_k\}$	heat maps
\mathbf{f}	convolutional feature maps
$\{\mathbf{H}_k\} = \mathcal{N}_H(\mathbf{f})$	heat map network
$\{\mathbf{J}_k\} = \mathcal{N}_J(\mathbf{f})$	joint network
$\{\mathbf{J}_k\} = \mathcal{I}(\{\mathbf{H}_k\})$	integral representation

Table 1. Notations.

In the wild pose estimation Most approaches work on the single person pose estimation problem [2]. The pose estimation ‘in the wild’ problem is more challenging, where the number of persons and their bounding boxes are not provided. It combines the problem of person detection with the problem of pose estimation. The recently released COCO person keypoints detection dataset and associated challenge [23] provide a challenging benchmark for this task.

There are two categories of methods for this problem. The *bottom-up* methods [34, 19, 5] firstly detect individual joints or body parts, and then assemble parts into person instances. The *top-down* methods [31, 16] firstly detect the persons and then perform single pose estimation in the bounding boxes. We follow a similar top-down paradigm as in [31].

3. Heat Map Based Methods

Such methods output a two dimensional heat map \mathbf{H}_k for k^{th} joint. Each location in the map represents the probability of the location being the joint, conforming to the *classification* paradigm. The joint is then obtained as the location with maximum likelihood as

$$\mathbf{J}_k = \arg \max_{\mathbf{p}} \mathbf{H}_k(\mathbf{p}). \quad (1)$$

This approach is simple and easy to train. However, it has a few drawbacks. First, Eq. (1) is *not-differentiable*, making it a post-processing step but not a component of learning. The training is not end-to-end. The semantic gap between the learning (heatmap estimation) and the target (joint estimation) is a fundamental limitation.

Second, the heat map representation leads to *quantization error*. The heat map resolution is much smaller than the input image resolution due to the down sampling steps in a deep neural network. The joint localization precision is thus limited by the quantization factor. For example, $8 \times$ down sampling is the typical setting in [43, 5, 34, 19, 40, 4]. A 256×256 input image generates 32×32 heat maps. The localization accuracy is no more than 4 pixels. This poses challenges for accurate joint localization. Using larger heat maps could alleviate this problem, but also introduce extra computational cost.

Last and most importantly, a heat map usually present *multiple local modes*. The ambiguity makes the joint prediction using Eq. (1) unstable and error-prone. Some examples are illustrated in Figure. 2. This is because heat map learning is essentially a dense per-pixel (or per-patch) classification problem. The classifiers are translation invariant and cannot distinguish locally similar image patches.

To alleviate above problems, state-of-the-art methods [43, 5, 29, 4, 15, 19, 12, 10, 8, 32] adopt a common multi-stage architecture. The predicted heat maps of each stage are used as input to the learning of next stage. In this way, the contextual information between heat maps of different joints is exploited to reduce the ambiguity and improve the heat map accuracy, gradually as more stages are used. Usually, a complex network is needed for high accuracy. See Table 7 for examples.

Methodology of experimental validation Existing state-of-the-art approaches [19, 43, 4, 29, 12, 10, 8] are quite complex (both in network structure and hyper-parameters) and hard to reproduce. The high complexity is adverse to clear idea validation and fair experimental comparison.

To facilitate ablation study and demonstrate the generality of our approach, this work adopts simple baselines in experiments. In spite of the simplicity, our baselines actually achieve strong performance (see Table 6) and serve as strong references for valid comparison.

We use a simple network architecture that is widely adopted in other vision tasks like object detection and segmentation [17, 16]. It consists of a deep convolutional *backbone* network to extract convolutional features \mathbf{f} from the input image, and a shallow *head* network to estimate the target output (heat maps or joints) from the features \mathbf{f} .

In this work, we adopt ResNet [17] as the backbone network. The input image size is normalized to 256×256 . The convolutional features are from conv5 block and of size 8×8 . All comparisons in this work, therefore, are based on different *head* networks.

Our baseline implementation For heat map estimation, the head network is denoted as \mathcal{N}_H ,

$$\mathbf{H}_k = \mathcal{N}_H(\mathbf{f}). \quad (2)$$

\mathcal{N}_H is fully convolutional. It firstly use 2 deconvolution layers (4×4 kernel, stride 2) to upsample the feature map from 8×8 to 32×32 . The number of output channels is fixed to 256 as in [16]. Then, a 1×1 conv layer is used to produce K heat maps. Batch normalization [20] and ReLU non-linearity [28] are used.

In the literature, there has been several choices for the loss function for the heat maps. The most widely adopted is mean square error (or L2 distance) between the predicted heat map and ground-truth heat map with a 2D

Gaussian blob centered on the ground truth joint location [41, 43, 5, 29, 8, 10, 12, 4]. In this work, the Gaussian blob has standard deviation $\sigma = 1$ as in [29]. Our baseline with this loss is denoted as H1 (H for heatmap).

The recent Mask RCNN work [16] uses a one-hot $m \times m$ ground truth mask where only a single location is labeled as joint. It uses the cross-entropy loss over an m^2 -way softmax output ($m = 32$ in this work). Our baseline with this loss is denoted as H2.

Another line of works [34, 19, 31] solve a per-pixel binary classification problem, thus using binary cross entropy loss. Each location in each heat map is classified as a joint or not. Following in [34, 19], the ground truth heat map for each joint is constructed by assigning a positive label 1 at each location within 15 pixels to the ground truth joint, and negative label 0 otherwise. Random negative samples are selected to keep the pos/neg ratio as 1 : 3. Our baseline with this implementation is denoted as H3.

We also use a simple multi-stage implementation. Based on ResNet-50, the 32×32 features from conv3 block are shared as input to all stages. Each stage then concatenates this feature with the heat maps from the previous stage, and pass through the conv4 and conv5 blocks to generate its own deep feature. The heat map head \mathcal{N}_H is then appended to output heat maps, supervised with the ground truth and losses. This supervision on the intermediate heat maps proves crucial for successful training [43, 29].

Details are shown in Figure. 1. Depending on the loss function used on the heat map, this multi-stage baseline is denoted as MS-H1(2,3).

4. Direct Joint Regression Methods

Such methods apply a head network \mathcal{N}_J to directly output a joint from the features,

$$\mathbf{J}_k = \mathcal{N}_J(\mathbf{f}). \quad (3)$$

Regression methods have two clear advantages over heat map based methods. First, learning is *end-to-end* and driven by the goal of joint prediction. There is no gap between learning and inference. Specifically, there is no post-processing and no multi-mode problem as in heat maps. Second, the output is *continuous* and up to arbitrary localization accuracy, in principle. This is opposed to the quantization problem in heat maps.

Regression methods are widely used for 3D pose estimation [38, 45, 46, 25, 27, 24, 30, 39]. This is partially attributed to that the 3D heat maps are impractical due to its demanding computation and storage cost.

Regression methods are less popular for 2D pose estimation [42, 6, 38]. The reasons are on both sides. On one hand, regression learning is inherently more difficult than heat map (classification) learning. The latter is supervised

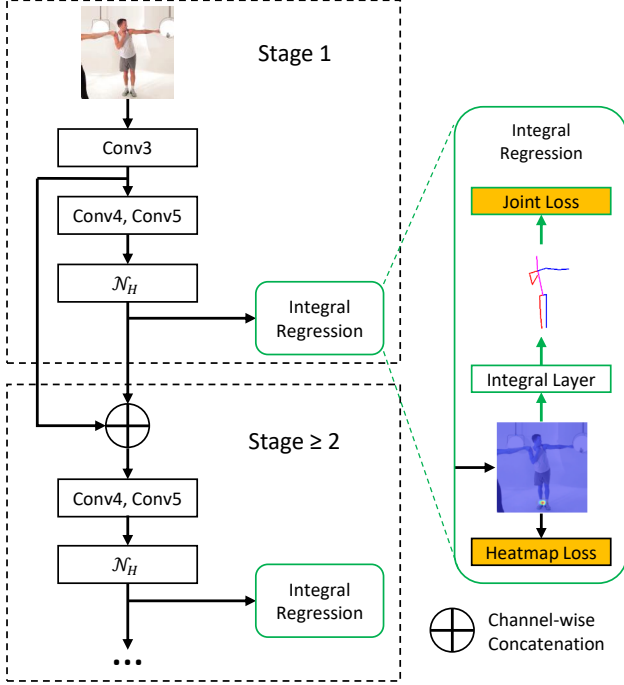


Figure 1. ResNet-50 based multi-stage architecture with or without integral regression. Arrows indicate data flow. Boxes are network layers. Network in *black* only is the baseline multi-stage architecture MS-H1(2,3). Network combining *black* and *green* is the integral regression version MS-II(2,3).

by dense pixel information and easier to train. On the other hand, the multi-stage architecture is crucial for good performance. The heat maps naturally have the convolutional representation and are easy to manipulate. It is much harder to adopt joint representation in a multi-stage network [6].

As a result, the leading approaches for 2D pose estimation are all heat map based [2, 1].

Our baseline implementation The head network \mathcal{N}_J follows [6, 38, 45, 46]. First, an average pooling layer reduces the spatial dimensionality of the convolutional features \mathbf{f} . Then, a fully connected layer output $2K$ joint coordinates. We experimented with both $L1$ and $L2$ distances between the predicted joints to ground truth joints as loss functions. We found that $L1$ loss works consistently better than $L2$ loss. We thus adopt $L1$ loss and denote our baseline as R1 (R for regression).

5. Integral Pose Regression

We present a unifying approach that possesses the merits of heat map and joint representation and avoids their drawbacks. Our approach simply modifies the *max* operation in Eq. (1) to take expectation, as

$$\mathbf{J}_k = \int_{\mathbf{p} \in \Omega} \mathbf{p} \cdot \tilde{\mathbf{H}}_k(\mathbf{p}). \quad (4)$$

Here, $\tilde{\mathbf{H}}_k$ is the normalized heat map and Ω is its domain. The estimated joint is the integration of all locations \mathbf{p} in the domain, weighted by their probabilities.

For normalization, we use softmax as

$$\tilde{\mathbf{H}}_k(\mathbf{p}) = \frac{e^{\mathbf{H}_k(\mathbf{p})}}{\int_{\mathbf{q} \in \Omega} e^{\mathbf{H}_k(\mathbf{q})}}. \quad (5)$$

The discrete form of Eq. (4) is

$$\mathbf{J}_k = \sum_{p_y=1}^H \sum_{p_x=1}^W \mathbf{p} \cdot \tilde{\mathbf{H}}_k(\mathbf{p}), \quad (6)$$

where (H, W) is the heat map dimension.

For notation clarify, the functions in Eq. (4), (5) and (6) are represented as a single integral function

$$\mathbf{J}_k = \mathcal{I}(\mathbf{H}_k). \quad (7)$$

In this way, any heat map based approach can be augmented for joint estimation by appending the integral function in Eq. (7) to the heat map \mathbf{H}_k and adopting a regression loss for \mathbf{J}_k . We call this approach *integral pose regression*.

For example, by combining Eq. (2) and (7), we have

$$\mathbf{J}_k = \mathcal{I}(\mathcal{N}_H(\mathbf{f})). \quad (8)$$

In this way, our heat map based baselines (MS-)H1, (MS-)H2, (MS-)H3 in Section 3 are upgraded to their integral regression version, called (MS-)I1, (MS-)I2, (MS-)I3, respectively. The joint loss is $L1$ distance, as in Section 4.

Integral pose regression shares all the merits of both heat map based and regression approaches. The integral function in Eq. (7) is differentiable and allow end-to-end training. It is simple, fast and brings no extra parameters. It can be easily combined with any heat map based methods, while adding little overhead in computation and memory for both training and inference. Its underlying heat map representation makes it easy to train. It has continuous output and does not suffer from the multi-mode problem.

6. Experiments

6.1. Experiments on MPII

MPII [3] is the benchmark dataset for single person 2D pose estimation. The images were collected from YouTube videos, covering daily human activities with complex poses and image appearances. There are about 25k images. In total, about 29k annotated poses are for training and another 7k are for testing.

method	@0.5	@0.1	AUC
H1	86.8	17.2	52.9
H2	86.4	17.6	53.1
H3	83.0	12.6	46.3
R1	84.6	25.0	54.1
I1	87.3	29.3	58.3
I2	86.9	29.7	58.3
I3	86.6	29.1	57.7
I*	86.0	28.3	56.6

Table 2. Comparison between methods using heat maps (Section 3), direct regression (Section 4), and integral regression (Section 5) on MPII validation set. Backbone network is ResNet-50.

Training We use the state-of-the-art ResNet [17] as backbone network. It is pre-trained on ImageNet classification dataset [14]. Adam [21] is used for optimization. In all experiments, the base learning rate is $1e-3$. It drops to $1e-5$ when the loss on the validation set saturates. Each method is trained with enough number of iterations until performance on validation set saturates. Mini-batch size is 128. Four GPUs are used. Batch-normalization [20] is used. Implementation is in MxNet [7].

The input image is normalized to 256×256 . Data augmentation includes random rotation (± 30 degrees), scaling ($\pm 25\%$) and flip.

For integral regression methods (I1, I2, I3, and their multi-stage version), the network is pre-trained only using heat map loss (thus their H versions) and then both losses on heat map and joint are used. We found this training strategy working slightly better than training from scratch using both losses.

Evaluation metric For performance evaluation, MPII [3] uses PCKh metric, which is the percentage of correct keypoint. A keypoint is correct if its distance to the ground truth is less than a fraction α of the head segment length. The metric is denoted as PCKh@ α .

Commonly, PCKh@0.5 metric is used for comparison [2]. For evaluation under high localization accuracy, which is also the strength of regression methods, we also report PCKh@0.1 and AUC (area under curve, the averaged PCKh when α varies from 0 to 0.5) metrics in all our ablation study.

Since the annotation on test set is not available, all our ablation studies are evaluated on an about $3k$ validation set which is separated out from the training set, following previous common practice [29]. Training is performed on the remaining training data.

Effect of integral regression Table 2 presents a comprehensive comparison. We first note that all integral regres-

sion methods (I1, I2, I3) clearly outperform their heat map based counterpart (H1, H2, H3). The improvement is especially significant on PCKh@0.1 with high localization accuracy requirement. For example, the improvement of I1 from H1 is +0.5 on PCKh@0.5, but +12.1 on PCKh@0.1. The overall improvement on AUC is significant (+5.4). Between the three heat map based methods, H3 performs worst. After using integral regression (I3), it is greatly improved, e.g., AUC from 46.3 to 57.7 (+11.4). Such results show that *joint training of heat maps and joint is effective*. The significant improvement localization accuracy (PCKh@0.1 metric) is attributed to the joint regression representation. Figure 2 shows that the heat map generated with integral regression is cleaner and less ambiguous.

We then investigate the effect of joint training. Towards that purpose, a variant of integral regression method is used, denoted as I*. The network is the same, but the loss on the heat maps is not used. The training supervision signal is only on joint, not on heat maps. Surprisingly, I* performs quite well. It is only slightly worse than I1/I2/I3 methods. It outperforms H1/H2/H3 on PCKh@0.1 and AUC, thanks to its regression representation. It outperforms R1, indicating the integral regression is better than direct regression, as both methods use exactly the same supervision and almost the same network (actually R1 has more parameters).

From above comparison, we can draw two conclusions. First, integral regression using an underlying heat map representation is effective ($I^* > H$, $I^* > R$). It works even without supervision on the heat map. Second, joint training of heat maps and joint combine the benefits of two paradigms and works best ($I > H, R, I^*$).

As H1 and I1 perform best, they are used in the remaining experiments. Figure 3 further shows the PCKh curves of H1, R1, I* and I1 for better illustration.

Effect of resolution Table 3 compares the results using two input image sizes and two output heat map sizes.

Not surprisingly, using large image size and heat map size obtains better accuracy, under all cases. However, integral regression (I1) is much less affected by the resolution than heat map based method (H1). It is thus a favorable choice when computational complexity is crucial and a small resolution is in demand.

For example, when heat map is downsized by half on image size $256 (c \text{ to } d)$, 1.1 G FLOPs (relative 15%) is saved. I1 only drops 0.6 in AUC while H1 drops 4.8. This gap is more significant on image size $128 (a \text{ to } b)$. 0.3G FLOPs (relative 17%) is saved. I1 only drops 3.5 in AUC while H1 drops 12.5.

When image is downsized by half ($d \text{ to } b$), 4.7 G FLOPs is saved (relative 76%). I1 only drops 11.1 in AUC while H1 drops 18.8.

Thus, we conclude that *integral regression significantly*



Figure 2. Heat map of right ankle (top row), left ankle (middle row) and right wrist (bottom row) generated by H1 (middle column) and I1 (right column)

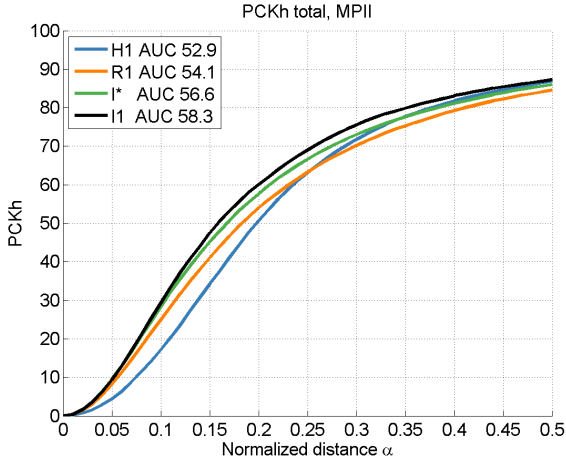


Figure 3. Curves of PCKh@ α of different methods while α varies from 0 to 0.5.

alleviates the problems of quantization error or needs of large resolution in heat map based methods.

Effect of network capacity Table 4 shows results using different backbone networks on three methods. While all methods are improved using a network with large capacity, integral regression I1 keeps outperforming heat map based method H1 and direction regression R1.

While a large network improves accuracy, a high complexity is also introduced. Integral regression I1 using

	$\times 2, \times 2, \times 2$	$\times 2, \times 2$
$128 \rightarrow 4$	$(a) \rightarrow 8 \rightarrow 16 \rightarrow 32$	$(b) \rightarrow 8 \rightarrow 16$
H1	81.6 / 13.6 / 46.6	75.4 / 5.6 / 34.1
I1	83.2 / 20.6 / 50.7	80.9 / 16.1 / 47.2
FLOPs	1.8G	1.5G
params	26M	26M
$256 \rightarrow 8$	$(c) \rightarrow 16 \rightarrow 32 \rightarrow 64$	$(d) \rightarrow 16 \rightarrow 32$
H1	86.7 / 28.0 / 57.7	86.8 / 17.2 / 52.9
I1	86.6 / 32.1 / 58.9	87.3 / 29.3 / 58.3
FLOPs	7.3G	6.2G
params	26M	26M

Table 3. For two methods (H1/I1), two input image \rightarrow feature map (f) resolutions, and two heat map sizes (using either 3 or 2 up-sampling layers), the performance metric (mAP@0.5, mAP@0.1, AUC), the computation (in FLOPs) and the amount of network parameters. Note that setting (d) is used in all other experiments.

ResNet-18 already achieves comparable accuracy with H1 and R1 using ResNet-101. This makes it a better choice when a small network is in favor, in practical scenarios.

Effect in multi-stage Table 5 shows the results of our multi-stage implementation with or without using integral regression. There are two conclusions. First, integral regression can be effectively combined with a multi-stage architecture and performance improves as stage increases. Second, integral regression outperforms its heat map based

	ResNet-18	ResNet-50	ResNet-101
H1	85.5 / 15.7 / 50.8	86.8 / 17.2 / 52.9	87.3 / 17.3 / 53.3
R1	82.4 / 21.9 / 50.8	84.6 / 25.0 / 54.1	85.7 / 26.9 / 55.6
I1	86.0 / 25.7 / 55.6	87.3 / 29.3 / 58.3	87.9 / 30.3 / 59.0
FLOPs	2.8G	6.2G	11.0G
params	12M	26M	45M

Table 4. PCKh@0.5, PCKh@0.1 and AUC metrics (top) of three methods, and model complexity (bottom) of three backbone networks. Note that ResNet-50 is used in all other experiments.

stage	MS-H1	MS-I1
1	86.8 / 17.2 / 52.9	87.3 / 29.3 / 58.3
2	86.9 / 17.6 / 53.4	87.7 / 32.0 / 59.5
3	87.1 / 17.8 / 53.7	87.8 / 32.4 / 59.9
4	87.4 / 17.8 / 54.0	88.1 / 32.3 / 60.1

Table 5. PCKh@0.5, PCKh@0.1 and AUC metrics of using and without using integral regression in a multi-stage network (see Section 3 for details).

counterpart on all stages. Specifically, MS-I1 stage-2 result 87.7 is already better than MS-H1 state-4 result 87.4.

From above ablation studies, we can conclude that *effectiveness of integral regression is attributed to its representation*. It works under different heat map losses (H1, H2, H3), different training (joint or not), different resolution, and different network architectures (depth or multi-stage).

Result on the MPII test benchmark Table. 6 summarizes the results of our methods, as well as state-of-the-art methods. In these experiment, our training is performed on all 29k training samples. We also adopt the flip test trick as used in [29]. Increasing the training data and using flip test would increase about 2.5 mAP@0.5 from validation dataset to test dataset.

We first note that our baselines has good performance, indicating they are valid and strong baselines. H1 and MS-H1 in the heat map based section has 89.4 and 89.8 PCKh, which are already comparable to many multi-stage methods, which are usually much more complex. R1 in regression section is already the best performing regression method.

Our integral regression further improves both baselines (I1>H1, MS-I1>MS-H1, 4 stages used) and achieve competitive results with respect to other methods.

While the accuracy of our approach is slightly below the state-of-the-art, we point out that the recent leading approaches [19, 43, 4, 29, 12, 10, 8] are all quite complex, making direct and fair comparison between these works difficult. Integral regression is simple, effective and can be combined with most other heat map based approaches, as validated in our baseline multi-stage experiments. Combination with these approaches is left as future work.

Method	Head	Sho.	Elb.	Wri.	Hip	Knee	Ank.	Mean
Pishchulin [33]	74.3	49.0	40.8	34.1	36.5	34.4	35.2	44.1
Tompson [41]	95.8	90.3	80.5	74.3	77.6	69.7	62.8	79.6
Tompson [40]	96.1	91.9	83.9	77.8	80.9	72.3	64.8	82.0
Hu [18]	95.0	91.6	83.0	76.6	81.9	74.5	69.5	82.4
Pishchulin [34]	94.1	90.2	83.4	77.3	82.6	75.7	68.6	82.4
Lifshitz [22]	97.8	93.3	85.7	80.4	85.3	76.6	70.2	85.0
Gkioxary [15]	96.2	93.1	86.7	82.1	85.2	81.4	74.1	86.1
Raf [35]	97.2	93.9	86.4	81.3	86.8	80.6	73.4	86.3
Insafutdinov [19]	96.8	95.2	89.3	84.4	88.4	83.4	78.0	88.5
Wei [43]	97.8	95.0	88.7	84.0	88.4	82.8	79.4	88.5
Bulat [4]	97.9	95.1	89.9	85.3	89.4	85.7	81.7	89.7
Newell [29]	98.2	96.3	91.2	87.1	90.1	87.4	83.6	90.9
Chu [12]	98.5	96.3	91.9	88.1	90.6	88.0	85.0	91.5
Chou [10]	98.2	96.8	92.2	88.0	91.3	89.1	84.9	91.8
Chen [8]	98.1	96.5	92.5	88.5	90.2	89.6	86.0	91.9
Ours: H1	97.9	95.3	90.0	85.5	88.3	85.3	80.7	89.4
Ours: MS-H1	98.0	95.4	90.2	86.3	88.1	85.8	82.1	89.8
Carreira [6]	95.7	91.7	81.7	72.4	82.8	73.2	66.4	81.3
Sun [38]	97.5	94.3	87.0	81.2	86.5	78.5	75.4	86.4
Ours: R1	97.8	95.2	87.6	80.3	89.6	80.7	73.0	87.0
Ours: I1	98.1	96.0	90.4	85.7	90.1	85.8	81.0	90.0
Ours: MS-I1	98.2	96.1	91.0	86.5	89.9	86.2	82.3	90.4

Table 6. Comparison to state-of-the-art works on MPII (top: heat map based, middle: regression based, bottom: integral regression). PCKh 0.5 metric is used.

method	PCKh	image size	params	FLOPs
CPM [43]	88.5	368 × 368	51M	134G
HG [29]	90.9	256 × 256	59M	73G
Ours: I1	90.0	256 × 256	26M	6.2G
Ours: MS-I1	90.4	256 × 256	101M	18G

Table 7. Overall comparison of several state-of-the-art methods and ours. HG [29] has 8 stages. CPM [43] has 6 stages. MS-I1 has 4 stages.

Table 7 further compares our approach with two representative multi-stage methods in terms of model complexity and accuracy. Compared to these multi-stage methods, the integral regression method I1 achieves comparable accuracy using fewer parameters and much less computation, e.g., 10× smaller than [29] and 20× smaller than [43].

6.2. Experiments on COCO

The COCO Keypoint Challenge [23] requires localization of person keypoints in challenging, uncontrolled conditions. The COCO train, validation, and test sets, containing more than 200k images and 250k person instances labeled with keypoints. 150k instances of them are publicly available for training and validation. Our models are trained on all COCO *trainval* samples and report the evaluation result on *test-dev* to make a fair comparison with the public state-of-the-art results [5, 16, 31]. The COCO evaluation defines the object keypoint similarity (OKS) and uses the mean average precision (AP) over 10 OKS thresholds as main competition metric [1]. The OKS plays the same role as the IoU in object detection. It is calculated from the distance be-

	backbone	AP^{kp}	AP_{50}^{kp}	AP_{75}^{kp}	AP_M^{kp}	AP_L^{kp}
CMU-Pose [5]		61.8	84.9	67.5	57.1	68.2
Mask R-CNN [16]	ResNet-50-FPN	63.1	87.3	68.7	57.8	71.4
G-RMI [31]	ResNet-101(353 × 257)	64.9	85.5	71.3	62.3	70.0
Ours: H1	ResNet-101(256 × 256)	66.3	88.4	74.6	62.9	72.1
Ours: I1	ResNet-101(256 × 256)	67.8	88.2	74.8	63.9	74.0

Table 8. COCO test-dev results.

tween predicted points and ground truth points normalized by scale of the person.

Person box detection We follow a two-stage top-down paradigm similar as in [31]. For human detection, we use Faster-RCNN [36] equipped with deformable convolution [13]. We use Xception [9] as the backbone network. The box detection AP on COCO test-dev is 0.49. For reference, this number in [31] is 0.487. Thus, the person detection performance is similar.

Following [31], we use the keypoint-based Non-Maximum-Suppression (NMS) mechanism building directly on the OKS metric to avoid duplicate pose detections. We also use the pose rescoring technique [31] to compute a refined instance confidence estimation that takes the keypoint heat map score into account.

Pose estimation We experimented with heat map based method (H1) in Section 3 and our integral regression methods (I1) in Section 5. Different from the experiments on MPII dataset, we use ResNet-101 as our backbone and use 3 deconvolution layers (4×4 kernel, stride 2) to upsample the feature maps. All the other settings are the same as experiments on MPII.

Results Table 8 summarizes the results of our methods, as well as state-of-the-art on COCO test-dev dataset. Our experiments are performed on COCO training data, no extra data is added. The baseline model (H1) is a one-stage ResNet-101 architecture. Our baseline model H1 is already superior to the state of the art top-down method [31]. Our integral regression further increases AP^{kp} by 1.5 points and achieve the state-of-the-art result.

7. Conclusion

We present a simple and effective integral regression approach that unifies the heat map representation and joint regression approaches, thus sharing the merits of both. Solid experiment results validate the efficacy of the approach. Strong performance is obtained using simple and cheap baseline networks, making our approach a favorable choice in practical scenarios.

Acknowledgement

We gratefully acknowledge the support of parallel deep learning training architecture from NVAITC (NVIDIA AI Tech Centre) for our research in Microsoft, Beijing.

References

- [1] COCO Leader Board. <http://cocodataset.org>. 4, 7
- [2] MPII Leader Board. <http://human-pose.mpi-inf.mpg.de>. 1, 2, 4, 5
- [3] M. Andriluka, L. Pishchulin, P. Gehler, and B. Schiele. 2d human pose estimation: New benchmark and state of the art analysis. In *Proceedings of the IEEE Conference on computer Vision and Pattern Recognition*, pages 3686–3693, 2014. 4, 5
- [4] A. Bulat and G. Tzimiropoulos. Human pose estimation via convolutional part heatmap regression. In *European Conference on Computer Vision*, pages 717–732. Springer, 2016. 1, 2, 3, 7
- [5] Z. Cao, T. Simon, S.-E. Wei, and Y. Sheikh. Realtime multi-person 2d pose estimation using part affinity fields. *arXiv preprint arXiv:1611.08050*, 2016. 1, 2, 3, 7, 8
- [6] J. Carreira, P. Agrawal, K. Fragkiadaki, and J. Malik. Human pose estimation with iterative error feedback. In *Proceedings of the IEEE Conference on Computer Vision and Pattern Recognition*, pages 4733–4742, 2016. 2, 3, 4, 7
- [7] T. Chen, M. Li, Y. Li, M. Lin, N. Wang, M. Wang, T. Xiao, B. Xu, C. Zhang, and Z. Zhang. Mxnet: A flexible and efficient machine learning library for heterogeneous distributed systems. *arXiv preprint arXiv:1512.01274*, 2015. 5
- [8] Y. Chen, C. Shen, X.-S. Wei, L. Liu, and J. Yang. Adversarial posenet: A structure-aware convolutional network for human pose estimation. *arXiv preprint arXiv:1705.00389*, 2017. 1, 2, 3, 7
- [9] F. Chollet. Xception: Deep learning with depthwise separable convolutions. *arXiv preprint arXiv:1610.02357*, 2016. 8
- [10] C.-J. Chou, J.-T. Chien, and H.-T. Chen. Self adversarial training for human pose estimation. *arXiv preprint arXiv:1707.02439*, 2017. 1, 2, 3, 7
- [11] X. Chu, W. Ouyang, H. Li, and X. Wang. Structured feature learning for pose estimation. In *Proceedings of the IEEE Conference on Computer Vision and Pattern Recognition*, pages 4715–4723, 2016. 1

- [12] X. Chu, W. Yang, W. Ouyang, C. Ma, A. L. Yuille, and X. Wang. Multi-context attention for human pose estimation. *arXiv preprint arXiv:1702.07432*, 2017. 1, 2, 3, 7
- [13] J. Dai, H. Qi, Y. Xiong, Y. Li, G. Zhang, H. Hu, and Y. Wei. Deformable convolutional networks. *arXiv preprint arXiv:1703.06211*, 2017. 8
- [14] J. Deng, W. Dong, R. Socher, L.-J. Li, K. Li, and L. Fei-Fei. Imagenet: A large-scale hierarchical image database. In *Computer Vision and Pattern Recognition, 2009. CVPR 2009. IEEE Conference on*, pages 248–255. IEEE, 2009. 5
- [15] G. Gkioxari, A. Toshev, and N. Jaitly. Chained predictions using convolutional neural networks. In *European Conference on Computer Vision*, pages 728–743. Springer, 2016. 1, 2, 3, 7
- [16] K. He, G. Gkioxari, P. Dollar, and R. Girshick. Mask r-cnn. In *International Conference on Computer Vision*, 2017. 1, 2, 3, 7, 8
- [17] K. He, X. Zhang, S. Ren, and J. Sun. Deep residual learning for image recognition. In *Proceedings of the IEEE Conference on Computer Vision and Pattern Recognition*, pages 770–778, 2016. 3, 5
- [18] P. Hu and D. Ramanan. Bottom-up and top-down reasoning with hierarchical rectified gaussians. In *Proceedings of the IEEE Conference on Computer Vision and Pattern Recognition*, pages 5600–5609, 2016. 7
- [19] E. Insafutdinov, L. Pishchulin, B. Andres, M. Andriluka, and B. Schiele. Deeppercut: A deeper, stronger, and faster multi-person pose estimation model. In *European Conference on Computer Vision*, pages 34–50. Springer, 2016. 1, 2, 3, 7
- [20] S. Ioffe and C. Szegedy. Batch normalization: Accelerating deep network training by reducing internal covariate shift. *arXiv preprint arXiv:1502.03167*, 2015. 3, 5
- [21] D. Kingma and J. Ba. Adam: A method for stochastic optimization. *arXiv preprint arXiv:1412.6980*, 2014. 5
- [22] I. Lifshitz, E. Fetaya, and S. Ullman. Human pose estimation using deep consensus voting. In *European Conference on Computer Vision*, pages 246–260. Springer, 2016. 7
- [23] T.-Y. Lin, M. Maire, S. Belongie, J. Hays, P. Perona, D. Ramanan, P. Dollár, and C. L. Zitnick. Microsoft coco: Common objects in context. In *European conference on computer vision*, pages 740–755. Springer, 2014. 1, 2, 7
- [24] J. Martinez, R. Hossain, J. Romero, and J. J. Little. A simple yet effective baseline for 3d human pose estimation. *arXiv preprint arXiv:1705.03098*, 2017. 3
- [25] D. Mehta, H. Rhodin, D. Casas, O. Sotnychenko, W. Xu, and C. Theobalt. Monocular 3d human pose estimation in the wild using improved cnn supervision. *arXiv preprint arXiv:1611.09813*, 2016. 3
- [26] T. B. Moeslund and E. Granum. A survey of computer vision-based human motion capture. *Computer vision and image understanding*, 81(3):231–268, 2001. 1
- [27] F. Moreno-Noguer. 3d human pose estimation from a single image via distance matrix regression. *arXiv preprint arXiv:1611.09010*, 2016. 3
- [28] V. Nair and G. E. Hinton. Rectified linear units improve restricted boltzmann machines. In *Proceedings of the 27th international conference on machine learning (ICML-10)*, pages 807–814, 2010. 3
- [29] A. Newell, K. Yang, and J. Deng. Stacked hourglass networks for human pose estimation. In *European Conference on Computer Vision*, pages 483–499. Springer, 2016. 1, 2, 3, 5, 7
- [30] B. X. Nie, P. Wei, and S.-C. Zhu. Monocular 3d human pose estimation by predicting depth on joints. In *Proc. IEEE Int. Conf. Comput. Vis.*, pages 3447–3455, 2017. 3
- [31] G. Papandreou, T. Zhu, N. Kanazawa, A. Toshev, J. Tompson, C. Bregler, and K. Murphy. Towards accurate multi-person pose estimation in the wild. *arXiv preprint arXiv:1701.01779*, 2017. 2, 3, 7, 8
- [32] G. Pavlakos, X. Zhou, K. G. Derpanis, and K. Daniilidis. Coarse-to-fine volumetric prediction for single-image 3d human pose. *arXiv preprint arXiv:1611.07828*, 2016. 1, 2, 3
- [33] L. Pishchulin, M. Andriluka, P. Gehler, and B. Schiele. Poselet conditioned pictorial structures. In *Proceedings of the IEEE Conference on Computer Vision and Pattern Recognition*, pages 588–595, 2013. 7
- [34] L. Pishchulin, E. Insafutdinov, S. Tang, B. Andres, M. Andriluka, P. V. Gehler, and B. Schiele. Deeppcut: Joint subset partition and labeling for multi person pose estimation. In *Proceedings of the IEEE Conference on Computer Vision and Pattern Recognition*, pages 4929–4937, 2016. 2, 3, 7
- [35] U. Rafi, I. Kostrikov, J. Gall, and B. Leibe. An efficient convolutional network for human pose estimation. In *BMVC*, volume 1, page 2, 2016. 7
- [36] S. Ren, K. He, R. Girshick, and J. Sun. Faster r-cnn: Towards real-time object detection with region proposal networks. In *Advances in neural information processing systems*, pages 91–99, 2015. 8
- [37] N. Sarafianos, B. Boteanu, B. Ionescu, and I. A. Kakadiaris. 3d human pose estimation: A review of the literature and analysis of covariates. *Computer Vision and Image Understanding*, 152:1–20, 2016. 1
- [38] X. Sun, J. Shang, S. Liang, and Y. Wei. Compositional human pose regression. In *International Conference on Computer Vision*, 2017. 2, 3, 4, 7
- [39] B. Tekin, P. Marquez Neila, M. Salzmann, and P. Fua. Learning to fuse 2d and 3d image cues for monocular body pose estimation. In *International Conference on Computer Vision (ICCV)*, number EPFL-CONF-230311, 2017. 3
- [40] J. Tompson, R. Goroshin, A. Jain, Y. LeCun, and C. Bregler. Efficient object localization using convolutional networks. In *Proceedings of the IEEE Conference on Computer Vision and Pattern Recognition*, pages 648–656, 2015. 2, 7
- [41] J. J. Tompson, A. Jain, Y. LeCun, and C. Bregler. Joint training of a convolutional network and a graphical model for human pose estimation. In *Advances in neural information processing systems*, pages 1799–1807, 2014. 3, 7
- [42] A. Toshev and C. Szegedy. Deeppose: Human pose estimation via deep neural networks. In *Proceedings of the IEEE Conference on Computer Vision and Pattern Recognition*, pages 1653–1660, 2014. 2, 3
- [43] S.-E. Wei, V. Ramakrishna, T. Kanade, and Y. Sheikh. Convolutional pose machines. In *Proceedings of the IEEE Conference on Computer Vision and Pattern Recognition*, pages 4724–4732, 2016. 1, 2, 3, 7

- [44] W. Yang, W. Ouyang, H. Li, and X. Wang. End-to-end learning of deformable mixture of parts and deep convolutional neural networks for human pose estimation. In *CVPR*, 2016. [2](#)
- [45] X. Zhou, Q. Huang, X. Sun, X. Xue, and Y. Wei. Towards 3d human pose estimation in the wild: a weakly-supervised approach. In *International Conference on Computer Vision*, 2017. [3](#), [4](#)
- [46] X. Zhou, X. Sun, W. Zhang, S. Liang, and Y. Wei. Deep kinematic pose regression. In *Computer Vision–ECCV 2016 Workshops*, pages 186–201. Springer, 2016. [3](#), [4](#)